

Article

# Stability Analysis and Trigger Control of LLC Resonant Converter for a Wide Operational Range

Zhijian Fang <sup>1</sup>, Junhua Wang <sup>1,\*</sup> , Shanxu Duan <sup>2</sup>, Jianwei Shao <sup>1</sup> and Guozheng Hu <sup>3</sup>

<sup>1</sup> School of Electrical Engineering, Wuhan University, Wuhan 430072, China; fangjianhust@gmail.com (Z.F.); hitwhshao@whu.edu.cn (J.S.)

<sup>2</sup> State Key Laboratory of Advanced Electromagnetic Engineering and Technology, School of Electrical and Electronic Engineering, Huazhong University of Science and Technology, Wuhan 430074, China; duanshanxu@hust.edu.cn

<sup>3</sup> School of Electrical and Electronic Engineering, Hubei Polytechnic University, Huangshi 435003, China; hgzh\_hs@163.com

\* Correspondence: junhuawang@whu.edu.cn; Tel.: +86-027-68776608

Academic Editor: Chunhua Liu

Received: 28 August 2017; Accepted: 12 September 2017; Published: 21 September 2017

**Abstract:** The gain of a LLC resonant converter can vary with the loads that can be used to improve the efficiency and power density for some special applications, where the maximum gain does not apply at the heaviest loads. However, nonlinear gain characteristics can make the converters unstable during a major disturbance. In this paper, the stability of an LLC resonant converter during a major disturbance is studied and a trigger control scheme is proposed to improve the converter's stability by extending the converter's operational range. Through in-depth analysis of the gain curve of the LLC resonant converter, we find that the switching frequency range is one of the key factors determining the system's stability performance. The same result is also obtained from a mathematical point of view by utilizing the mixed potential function method. Then a trigger control method is proposed to make the LLC resonant converter stable even during a major disturbance, which can be used to extend the converter's operational range. Finally, experimental results are given to verify the analysis and proposed control scheme.

**Keywords:** LLC resonant converter; stability; trajectory; mixed potential function; trigger control

## 1. Introduction

DC/DC converters have been widely used to provide constant voltage or current [1–4]. When the DC/DC converter is controlled as a voltage source, the voltage is constant and the current varies from zero to maximum value. When the converter is used as a current source, the current is constant and voltage varies from zero to maximum value. Therefore, the operation area is the rectangle where most converters work, such as battery charger, DC power supply, UPS, etc.

However, in some special applications, the voltage and current are not constant but vary with the loads. For example, the voltage–current curve of the plasma cutting is shown in Figure 1. In startup, the output voltage rises to maximum value slowly without output current, providing a high output voltage to build a strong electrical field to produce air plasma. Then the arc striking circuit begins to work and the air is broken down with a low resistance, making the output current rise and output voltage fall quickly. Finally, the output current is regulated to the desired value [5,6]. In these applications, the power supply's voltage falls as the current rises, leading to a concave operation area (shown in Figure 2), which is smaller than the rectangular area.

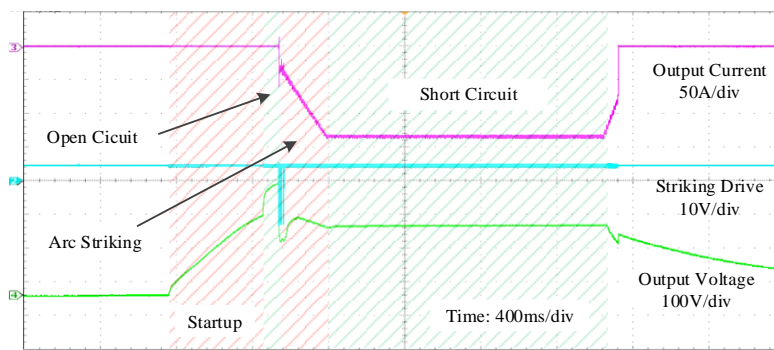


Figure 1. Waveforms of plasma arc cutting.

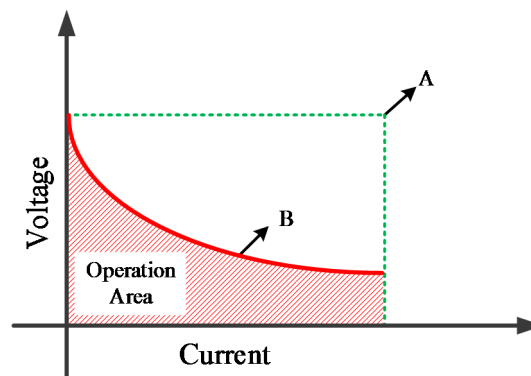


Figure 2. Operation area of special applications.

Most DC/DC converters are a linear system in which the output voltage or current is decided by control signals like duty cycle or phase shift, and are not influenced by the loads [7–9]. Therefore, the operation area of these converters is similar to a rectangle. When these converters are used to provide energy for some special applications, like plasma arc cutting, the operational area of the converters will be far larger than the requirements of the applications. In Figure 2, the maximum power needed by the application is at point B, but the maximum power the converters can generate is at point A. The redundant design could increase the converters' cost and volume. At the same time, the converter's efficiency is reduced.

In a resonant DC/DC converter, the output voltage or current will vary with the loads, even using the same switching frequency [10]. Figure 3 shows the gain curves of a LLC resonant converter under different load conditions [11–13]. When the switching frequency is fixed, the gain of the converter could fall as the loads increase, which means the output voltage of the resonant converter could fall as the current rises, similar to the operational area in Figure 2. If the resonant converter's operation area is designed to fit the operation area of the special applications, higher power density and efficiency of the resonant converters can be achieved.

In [14], the series-parallel resonant converter (SPRC) is used for the plasma arc cutting, achieving high power density and efficiency. The switching frequency is fixed at 125 kHz, which can achieve a high output voltage at open circuit and a very low voltage at short circuit. However, in this application the output currents can only be regulated by sliding the phase among multiple modules. For a single resonant converter module, the switching frequency must be regulated to control the output voltage and current. A simulation module of the LLC resonant converter is applied for the plasma arc cutting. A high output voltage, as large as 100 V at open circuit, and high output current, as large as 100 A at short circuit, can be achieved. The PI controller is used to regulate the switching frequency to control the output voltage and current. When the converter starts up at heavy loads, the output current can be regulated to 100 A, as shown in Figure 4a. When the converter starts up with no loads, the output

voltage can be regulated to 100 V, as shown in Figure 4b. The output voltage can be maintained at 100 V after 9 ms. At  $t = 10$  ms, a step load appears and the output current cannot be regulated to 100 A under the short circuit condition, making the converter unstable. In this special application, the converter can work stably despite a minor disturbance but becomes unstable when a major disturbance occurs.

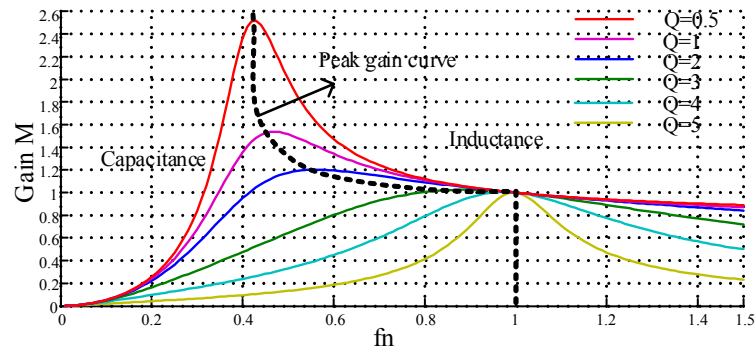


Figure 3. Gain curve of LLC resonant converter.

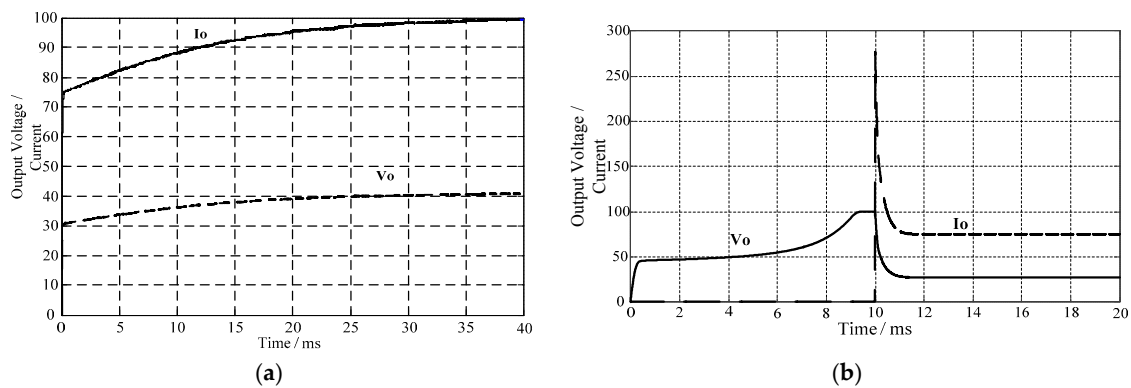


Figure 4. The waveforms of output voltage and current of the LLC resonant converter at different disturbance levels: (a) minor disturbance; (b) major disturbance.

In order to solve this problem, some studies have been published on the stability and control scheme of the LLC resonant converters [15,16]. The small-signal analysis method is the most popular and effective method [17–20]. An EDF-based nonlinear model is built, obtaining the linearized model at the equilibrium point by using the Lyapunov linearization method. Then the stability criterion is achieved based on the conventional stability analysis. The small-signal analysis method is quite effective and simple, and can be used when the system operates only near the equilibrium point. However, the occurrence of a major disturbance can render the small signal analysis method ineffective, such as the starting-up pulse or load transient, Therefore, the overall stability performance of the LLC resonant converter can only be guaranteed by small signal analysis and researchers need to propose improved methods to extend the application range. Jang et al. [21,22] calculated the stability criterion at the most serious condition to ensure the LLC resonant converter's stability. Zong et al. [23] linearized a nonlinear system through resonant current feedback and then used the small signal analysis method. There are also some nonlinear analysis methods, such as the phase plane, feedback linearization, and the Lyapunov direct method [15,24–26]. However, those methods cannot correctly achieve the attraction region and the stability criterion, limiting the applicability. These published papers pay little attention to the unstable phenomenon of the LLC resonant converter during a major disturbance, where the LLC resonant converter, which can maintain stability during a minor disturbance, may be unstable due to its nonlinear characteristics.

The main reason why conventional analysis and control methods do not work in these special applications is that the nonlinear characteristics used in these applications to improve the power density and efficiency make the conventional linear analysis and control methods fail. In this paper, the instability characteristics of the LLC resonant converter during major disturbance conditions are studied intensively. Through in-depth analysis of the gain curve of the LLC resonant converter, we find that the switching frequency range is one of the key factors determining the system stability performance of the LLC resonant converter. The regulated switching frequency should be higher than the critical frequency to ensure the stability of the system, or the converter will fall into instability. The same result is obtained from a mathematical point of view by the utilization of the mixed potential function method. After these analyses, a trigger control method is proposed to make the LLC resonant converter stable under major disturbance conditions, which can be used to support the resonant converter applied for the special applications.

The rest of this paper is organized as follows. In Section 2, the instability phenomenon of the LLC resonant converter is analyzed from the view of the gain curve. Then the mathematically derived process is expressed in Section 3, based on the mixed potential function method. In Section 4, a trigger control scheme is given to extend the operational range of the LLC resonant converter. The experimental results are shown in Section 5 to verify the proposed analysis and control methods, followed by conclusions in Section 6.

## 2. Instability Phenomenon

Figure 5 shows the circuit block diagram of the LLC resonant converter. The full bridge, consisting of four MOSFETs, produces a square wave voltage for the resonant tank, which is composed of a resonant inductor, capacitor, and magnetic inductor. The rectifier transfers the resonant AC voltage to DC voltage. Through varying the switching frequency, the resonant tank impedance can be adjusted and thus the output voltage can be controlled.

Generally, traditional PI controllers can be used in the LLC resonant converters for output voltage regulation, as shown in Figure 5. When the output voltage is higher than the reference value, the modulation voltage generated by the PI controller will increase and the voltage-to-frequency conversion will generate a higher switching frequency. Thus the resonant tank impedance will increase and the output voltage will decrease accordingly. Similarly, when the output voltage is lower than the reference voltage, the switching frequency will decrease and output voltage will increase. The output voltage can be regulated to the reference value through the conventional linear controller.

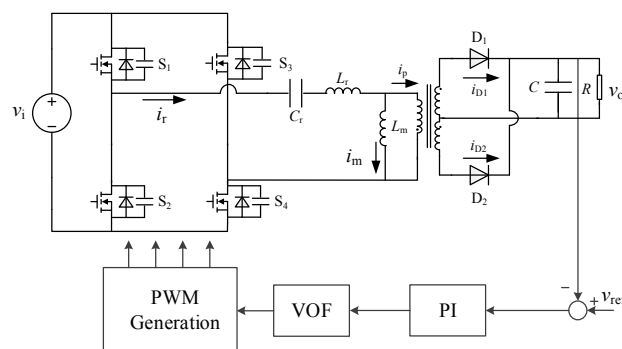
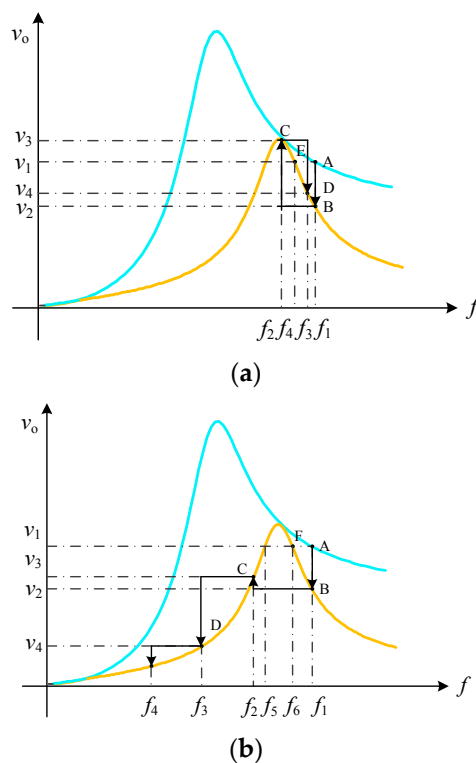


Figure 5. Circuit block diagram of LLC resonant converter.

According to the operation principle of the LLC resonant converter, it can be seen that the resonant tank impedance should be inductive to guarantee the stability of the LLC resonant converter. Otherwise, the resonant tank is capacitive. In this case, when the output voltage is higher than the reference value, the controller will regulate a higher switching frequency, which causes a higher output voltage. Then positive feedback occurs, regulating the output voltage to the maximum or minimum

value and causing the LLC resonant converter to become unstable. Unfortunately, the LLC resonant converter is a nonlinear system, and the resonant impedance may be capacitive or inductive depending on the switching frequency value. The gain curve of the LLC resonant converter is shown in Figure 3. When the converter operates in the inductive area, the output voltage will decrease as the frequency increases. When the converter operates in the capacitive area, the output voltage increases as the frequency increases.

Assume that the LLC resonant converter operates at point A, as shown in Figure 6a. The reference voltage is  $v_1$  and the switching frequency is  $f_1$ . When a minor disturbance occurs, the loads increase correspondingly and the output curve changes from the blue line to the yellow one, leading to a slight decrease in output voltage from  $v_1$  to  $v_2$  at frequency  $f_1$ , making the operation point move to point B. Then the output voltage is lower than the reference value, making the controller producing a lower switching frequency  $f_2$  and the operation point transfers to point C. The output voltage is  $v_3$  at point C, which is higher than the reference value,  $v_1$ . The frequency will be increased by the controller regulation to reduce the output voltage. The converter is regulated to work at point D. Finally, the converter will stably operate at a new point E, and at a new frequency  $f_4$ . During the whole regulating process, the converter operates in the inductive area. The converter can operate stably under minor disturbances.



**Figure 6.** Operation trajectory of LLC resonant converter under different disturbance conditions: (a) minor disturbance; (b) major disturbance.

However, the converter may go into the capacitive area during the controlling process, especially in major disturbance conditions. When major disturbances occur, the loads increase, as shown in Figure 6b. Due to the heavy step loads, the output voltage will be reduced to  $v_2$  at operation point B. Since the output voltage  $v_2$  is far smaller than the reference voltage,  $v_1$ , the large input error will produce a small switching frequency,  $f_2$ , making the converter operating at point C fall into the capacitive area. As the output voltage  $v_3$  at point C is still lower than reference value  $v_1$ , the controller will continue to decrease the switching frequency to  $f_3$ , which causes a lower output voltage due to the capacitive characteristics of the resonant tank. Then positive feedback occurs, making the converter

operate from point D to E and finally to the original point. The converter becomes unstable during a period of major disturbance. Therefore, the conventional linear stable analysis method cannot ensure the converter's stability during a major disturbance. It is necessary to analyze the stability of the LLC resonant converter during a major disturbance.

From the above analysis, it can be shown that a minor disturbance and slower controller regulating speed will make the converter more stable. When the converter operates in the inductive area during the whole regulating process, the converter can operate stably as in the normal design. Otherwise, the converter enters into the capacitive area, as shown in Figure 6b, and instability occurs. By observing Figure 6b, it can be seen that if the switching frequency is lower than  $f_5$ , the output voltage will be lower than the reference value, and the controller will reduce the frequency to increase the output voltage until the frequency is regulated to zero. If the frequency is higher than  $f_5$  and lower than  $f_6$ , the output voltage will be higher than the reference value and the controller will increase the frequency to reduce the output voltage. When the frequency is higher than  $f_6$ , the output voltage is lower than the reference voltage and the controller will reduce the frequency to increase the output voltage. Finally, the LLC resonant converter operates stably at point F. So  $f_5$  is the stable criterion of the LLC resonant converter at which the LLC resonant converter can generate a new reference voltage in the capacitive area. The stability criterion will vary with the loads and the reference and the minimum value will be obtained when the new reference voltage is equal to the peak value of LLC resonant converter's gain curve. We name the frequency achieving the peak gain the peak frequency. Thus, when the switching frequency is higher than the peak frequency during the whole controlling process, the converter can be guaranteed to operate stably during any disturbance. Otherwise, the converter may operate in the capacitive area and instability occurs. Thus the peak frequency is the critical condition for stable operation of the LLC resonant converter, which can be obtained as follows:

$$v_o = v_i/n\sqrt{(1+h-h/f^2)^2+Q^2(f-1/f)^2}, \quad (1)$$

where  $h$  is the inductor ratio ( $h = L_r/L_m$ ),  $Q$  is the quality factor ( $Q = \sqrt{L_r/C_r}/R_e$ ,  $R_e = 8n^2R/\pi^2$ ), and  $f$  is the normalized frequency  $f = \omega\sqrt{L_rC_r}$ . Then the peak frequency can be calculated:

$$\left.\frac{\partial v_o}{\partial f}\right|_{f=f_{peak}} = 0 \rightarrow Q^2f^6 + (2h^2 + 2h - Q^2)f^2 - 2h^2 = 0. \quad (2)$$

To ensure the stable operation of the LLC resonant converter, the frequency must be larger than the peak frequency during the whole regulation process. Otherwise, the converter will work in the capacitive area and be unstable.

### 3. Stability Analysis

In the previous section, the instability of the LLC resonant converter during a major disturbance was analyzed based on the operational trajectory of the LLC resonant converter. However, this was just a qualitative result. In this section, based on the extended describing function method, the control-to-output transfer function of the LLC resonant converter is derived. Then a stability analysis is also performed through the mixed potential function method.

#### 3.1. Modeling of LLC Resonant Converter

The LLC resonant converter has four state variables. The state equations can be obtained as follows:

$$\begin{aligned} L_r \frac{di_r}{dt} &= -v_m - v_{cr} + v_{ab} \\ L_m \frac{di_m}{dt} &= v_m \\ C_r \frac{dv_r}{dt} &= i_r \\ C_o \frac{dv_o}{dt} &= i_s - i_o \end{aligned}, \quad (3)$$

where  $i_r$ ,  $i_m$ ,  $v_r$ , and  $v_o$  are the resonant and magnetic current, and resonant and output voltage, respectively.  $v_m$  is the magnetic voltage and  $i_s$  is the average rectifier current at the secondary side.  $v_{ab}$  is the bridge voltage and  $i_o$  is the output current.

Since the switching frequency is close to the natural frequency of the resonant tank, the waveforms of resonant components are nearly sinusoidal. Resonant variables can be approximated by fundamental harmonics.

$$\begin{aligned} i_r &= i_{rs} \sin \omega t + i_{rc} \cos \omega t \\ i_m &= i_{ms} \sin \omega t + i_{mc} \cos \omega t, \\ v_r &= v_{rs} \sin \omega t + v_{rc} \cos \omega t \end{aligned} \quad (4)$$

where  $\omega$  is the switching angular frequency. Due to the large output capacitor  $C_o$ ,  $v_m$  is a square waveform voltage, similar to  $v_{ab}$ . Then the input state variables can be calculated:

$$\begin{aligned} v_{ab} &= \frac{4}{\pi} v_i \sin \omega t \\ v_m &= \frac{4}{\pi} \frac{i_{rs} - i_{ms}}{i_p} n v_o \sin \omega t + \frac{4}{\pi} \frac{i_{rc} - i_{mc}}{i_p} n v_o \cos \omega t, \\ i_p &= \sqrt{(i_{rs} - i_{ms})^2 + (i_{rc} - i_{mc})^2} \end{aligned} \quad (5)$$

where  $n$  is the transformer ratio and  $i_p$  is the peak value of rectifier current at the primary side. At the secondary side, all state variables are DC waveforms. The ripple waveform of the rectifier current can be ignored. Then the average current can be derived:

$$i_s = \frac{2}{\pi} n i_p. \quad (6)$$

By substituting Equations (4)–(6) into Equation (3), the state equations can be obtained. Since the control frequency is very low, the resonant variables can reach steady state during the control period. Then the coefficients of the sine and cosine terms can be calculated. The following equations can be used:

$$\begin{aligned} L_r \frac{di_{rs}}{dt} &= \omega L_r i_{rc} - v_{rs} - \frac{4}{\pi} \frac{i_{rs} - i_{ms}}{i_p} n v_o + \frac{4}{\pi} v_i \\ L_r \frac{di_{rc}}{dt} &= -\omega L_r i_{rs} - v_{rc} - \frac{4}{\pi} \frac{i_{rc} - i_{mc}}{i_p} n v_o \\ L_m \frac{di_{ms}}{dt} &= \omega L_m i_{mc} + \frac{4}{\pi} \frac{i_{rs} - i_{ms}}{i_p} n v_o \\ L_m \frac{di_{mc}}{dt} &= -\omega L_m i_{ms} + \frac{4}{\pi} \frac{i_{rc} - i_{mc}}{i_p} n v_o \\ C_r \frac{dv_{rs}}{dt} &= \omega C_r v_{rc} + i_{rs} \\ C_r \frac{dv_{rc}}{dt} &= -\omega C_r v_{rs} + i_{rc} \\ C_o \frac{dv_o}{dt} &= \frac{2}{\pi} n i_p - i_o \end{aligned} \quad (7)$$

The LLC resonant converter model is a seven-order nonlinear system, so it is difficult to analyze the characteristics of the LLC resonant converter based on this model. In Figure 6, it can be seen that the LLC resonant converter can be divided into a resonant part and a rectifier part. The output of the resonant part is the rectifier current,  $i_p$ . Combining Equations (5) and (7), the state equation of  $i_p$  can be derived as follows:

$$\begin{aligned} \frac{di_p}{dt} &= -\frac{4}{\pi} n v_o \left( \frac{1}{L_r} + \frac{1}{L_m} \right) + \frac{4}{\pi} v_i \frac{1}{L_r} \frac{i_{rs} - i_{ms}}{i_p} - \\ &\quad v_{rs} \frac{1}{L_r} \frac{i_{rs} - i_{ms}}{i_p} - v_{rc} \frac{1}{L_r} \frac{i_{rc} - i_{mc}}{i_p}. \end{aligned} \quad (8)$$

Usually, the resonant components in the LLC resonant converter are very small due to the high resonant frequency. Moreover, the output capacitor is designed to be very large to ensure steady output voltage. Meanwhile, the control frequency is much lower than the switching frequency. Then the resonant state variables can be regarded as steady state values during every control period. By substituting the steady values of resonant state variables, Equation (8) can be simplified as follows:

$$\frac{di_p}{dt} = -4(1/L_r + 1/L_m)n v_o / \pi + 4(1/L_r + 1/L_m)M v_i / \pi. \quad (9)$$

$M$  is the steady gain of the LLC resonant converter, which is expressed as follows:

$$M = 1/\sqrt{(1+h-h/f^2)^2 + Q^2(f-1/f)^2}. \quad (10)$$

The LLC resonant converter can be simplified as a two-order circuit, as shown in Figure 7.

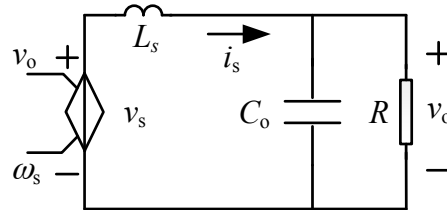


Figure 7. Equal two-order circuit of LLC resonant converter.

Then the state equations of LLC resonant converter can be derived as follows:

$$\begin{aligned} C_o \frac{dv_o}{dt} &= i_s - i_o \\ L_s \frac{di_s}{dt} &= v_s - v_o \end{aligned} \quad (11)$$

The equal output inductor can be derived as follows:

$$L_s = \pi^2 / [8n^2(1/L_r + 1/L_m)]. \quad (12)$$

$v_s$  is the equal input voltage, which is expressed as follows:

$$v_s = \sqrt{\frac{(v_i/n)^2/(1/f-f)^2 - (i_s\pi^2/8)^2 L_r/C_r}{[1/(1/f-f) - h/f]^2}}. \quad (13)$$

### 3.2. Stability Analysis of LLC Resonant Converter

A simplified model of the LLC resonant converter has been derived. However, it is still a nonlinear model, which means that conventional linear stability analysis methods are not suitable for the analysis. The small signal stability method can be applied to nonlinear systems, but it is insufficient to provide the overall stability that is a criterion of the LLC resonant converter. The Lyapunov stability theory has been widely used to achieve stability for nonlinear systems, but it is difficult to construct the Lyapunov energy function. Brayton and Moser proposed a mixed potential theory in 1964, which can be used to construct the energy function and achieve stability.

Mixed potential functions can describe the dynamic characteristics of the nonlinear RLC circuit. There must be a function in the RLC circuit that has the special forms as follows:

$$\begin{aligned} \mathbf{J} \cdot \dot{\mathbf{x}} &= \frac{\partial P(\mathbf{x})}{\partial \mathbf{x}} = \nabla P(\mathbf{x}) \\ \mathbf{x} &= \begin{bmatrix} \mathbf{i} \\ \mathbf{v} \end{bmatrix}, \quad \mathbf{J} = \begin{bmatrix} -\mathbf{L} & \mathbf{0} \\ \mathbf{0} & \mathbf{C} \end{bmatrix}, \end{aligned} \quad (14)$$

where  $\mathbf{i}$  is the inductor current and  $\mathbf{v}$  is the capacitor voltage in the circuit;  $P(\mathbf{x})$  is the mixed potential function. Since the function consists of current and voltage potential functions in the system, the mixed potential function  $P(\mathbf{x})$  can also be expressed as follows:

$$P(\mathbf{i}, \mathbf{v}) = A(\mathbf{i}) - B(\mathbf{v}) + N(\mathbf{i}, \mathbf{v}), \quad (15)$$

where  $A(\mathbf{i})$  is the current potential function related with the current-controlled resistors and the voltage source;  $B(\mathbf{v})$  is the voltage potential function related with the voltage-controlled resistors and the current source; and  $N(\mathbf{i}, \mathbf{v})$  is determined by the interconnection of the inductors and capacitors:

$$N(\mathbf{i}, \mathbf{v}) = \sum_{j=1}^l \sum_{k=1}^c \gamma_{jk} i_j v_k, \quad (16)$$

where  $i_j$  ( $j = 1, 2, \dots, l$ ) represents all the independent inductor currents;  $v_k$  ( $k = 1, 2, \dots, c$ ) represents all the independent capacitor voltages; and  $\gamma_{jk}$  is the inner connection between  $i_j$  and  $v_k$ , which can be 1, -1, or 0. The detailed derivation process is described in [27–29].

Several theorems on the stability of circuits have been derived and Theorem 5 will be used to analyze the stability of the LLC resonant converter. This theorem is restated as follows.

Suppose that  $\mu_1$  is the minimum eigenvalue of matrix  $\mathbf{K}_1$  for all inductor currents and  $\mu_2$  is the minimum eigenvalue of  $\mathbf{K}_2$  for all capacitor voltages. If all the inductors and capacitors are constant, matrix  $\mathbf{K}_1$  and  $\mathbf{K}_2$  are:

$$\begin{aligned} \mathbf{K}_1 &= \nabla^2 A(\mathbf{i}) \\ \mathbf{K}_2 &= \nabla^2 B(\mathbf{v}) \end{aligned} \quad (17)$$

Under the condition that

$$\mu_1 + \mu_2 \geq \delta, \quad \delta > 0 \quad (18)$$

for all currents and voltages and  $V(\mathbf{x}) \rightarrow \infty$  as  $|\mathbf{x}| \rightarrow \infty$ , all trajectories of Equation (14) tend to the set of equilibrium points as  $t \rightarrow \infty$ .

This part will analyze the stability of the LLC resonant converter based on the mixed potential theory. According to the model of the LLC resonant converter, the mixed potential function of the LLC resonant converter can be obtained as follows:

$$P(i_s, v_o) = - \int_0^{i_s} (Mv_i/n) di - \int_0^{v_o} i_o dv + i_s v_o. \quad (19)$$

Then all three parts of the mixed potential function can be achieved:

$$\begin{aligned} A(i_s) &= - \int_0^{i_s} (Mv_i/n) di \\ B(v_o) &= \int_0^{v_o} i_o dv \\ N(i_s, v_o) &= i_s v_o \end{aligned} \quad (20)$$

Then the minimum eigenvalue  $\mu_1$  and  $\mu_2$  can be calculated:

$$\begin{aligned} \mu_1 &= \nabla^2 A(i_s) = \frac{\partial^2 A(i_s)}{\partial i_s^2} = - \frac{\partial v_s}{\partial i_s} \\ \mu_2 &= \nabla^2 B(v_o) = \frac{\partial^2 B(v_o)}{\partial v_o^2} = \frac{\partial i_o}{\partial v_o} \end{aligned} \quad (21)$$

The input voltage  $v_s$  has been calculated in Equation (13). The PI controller is used in the LLC resonant converter to regulate the output voltage. The regulated switching frequency can be derived as follows:

$$\omega = k_p (v_{ref} - v_o) + k_i \int (v_{ref} - v_o) dt. \quad (22)$$

Then the eigenvalue  $\mu_1$  can be calculated:

$$\mu_1 = - \frac{\partial v_s}{\partial i_s} = -1 / \left( \frac{\partial i_s}{\partial v_s} \right). \quad (23)$$

Since  $v_s$  is near the output voltage  $v_o$ , the follow equation is given:

$$\frac{\partial \omega}{\partial v_s} \approx \frac{\partial \omega}{\partial v_o} = -k_p. \quad (24)$$

Based on the theorems mentioned earlier, the stability criterion of LLC resonant converter can be expressed as follows:

$$\mu_1 + \mu_2 = 1/R - \pi^2 \sqrt{L_r/C_r} \sqrt{[f/(1-f^2)]^2/M^2 - [f/(1-f^2) - h/f]^2} / 8n^2 / \left\{ \begin{array}{l} \left\{ \begin{array}{l} v_s(f+f^3)/M^2/(1-f^2)^3 - \\ v_s[f/(1-f^2) - h/f] \cdot [(1+f^2)/(1-f^2)^2 + h/f^2] \end{array} \right\} \cdot (-k_p) - \\ [f/(1-f^2) - h/f]^2 \end{array} \right\} > 0. \quad (25)$$

Since the LLC resonant converter must be stable no matter how heavy the load, the stability of the LLC resonant converter can be derived as follows:

$$0 > \left\{ \begin{array}{l} v_s(f+f^3)/M^2/(1-f^2)^3 - \\ v_s[f/(1-f^2) - h/f] [(1+f^2)/(1-f^2)^2 + h/f^2] \end{array} \right\} \cdot (-k_p). \quad (26)$$

Then it can be simplified:

$$(-k_p)v_s(-f^2)/(1-f^2)^2 \left[ \frac{Q^2(f-1/f)(1+1/f^2) + 2(1+h-h/f^2)h/f^3}{2(1+h-h/f^2)h/f^3} \right] < 0. \quad (27)$$

Since the input voltage  $v_s$  is positive, the criterion can be simplified as:

$$k_p \left[ Q^2(f-f^{-1})(1+f^{-2}) + 2(1+h-h/f^2)h/f^3 \right] < 0. \quad (28)$$

It is still difficult to guide the controller design. Obtaining the LLC resonant converter gain as described in Equation (10), we get the follow equation:

$$\frac{\partial M}{\partial f} = \frac{Q^2(f^{-1}-f)(1+f^{-2}) - 2(1+h-h/f^2)h/f^3}{\sqrt{Q^2(f-f^{-1})^2 + (1+h-h/f^2)^2}}. \quad (29)$$

The polarity of the converter gain's differential is the same as the stability criterion. We can make the following conclusions:

$$\begin{array}{l} \frac{\partial M}{\partial f} > 0, \quad \text{at } 0 < f < f_{peak} \\ \frac{\partial M}{\partial f} < 0, \quad \text{at } f_{peak} < f \end{array}. \quad (30)$$

From Equations (28)–(30), the stability criterion of the LLC resonant converter can be calculated as follows.

(1) range of the switching frequency is  $0 < f < f_{peak}$ , then the stability criterion is

$$k_p > 0, \quad \text{at } 0 < f < f_{peak}. \quad (31)$$

(2) If the variable range of the switching frequency is  $f_{peak} < f$ , then the stability criterion is

$$k_p < 0, \quad \text{at } f_{peak} < f. \quad (32)$$

According to Section 2, the proportion coefficient  $k_p$  of the conventional control scheme for the LLC resonant converter is negative. Then a higher input error of the controller can produce a lower switching frequency. Therefore, the stability criterion of LLC resonant converter is

$$f > f_{peak}. \quad (33)$$

This is the same as the analysis in Section 2, derived from the gain curve.

#### 4. Trigger Control Scheme

From the last section's analysis, the main reason for the LLC resonant converter's instability is that the converter works into the capacitance operation during a major disturbance. In order to make the LLC resonant converter stable, the converter must be forced to work into the inductance operation area after a major disturbance. Then a trigger control scheme is proposed with a current polar discriminator (CPD), as shown in Figure 8. The CPD samples the resonant current when the driving signal of switcher  $S_1$  rises from low to high. If the resonant current is negative, the LLC resonant converter works at inductance operation. Otherwise, operate at capacitance operation. When the LLC resonant converter works at capacitance operation, the CPD sends a trigger signal to the PI controller. Then the PI controller regulates the frequency to the peak frequency value and the LLC converter works at inductance operation again, making the converter stable. The PI controller can regulate the output voltage to the desired value.

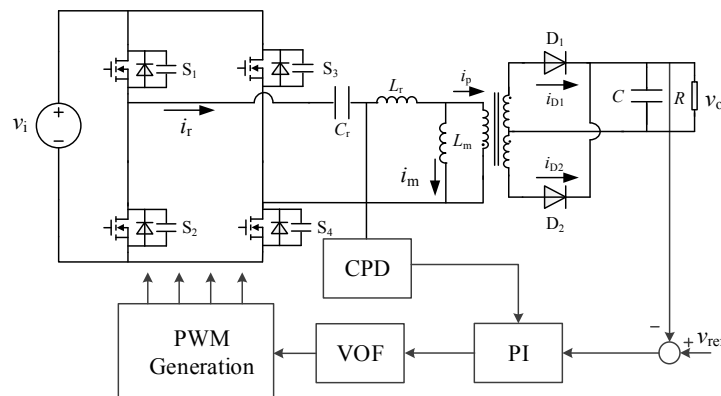


Figure 8. Trigger control scheme of the LLC resonant converter.

This proposed trigger control method is verified for the simulation model in Section 1. The output voltage is shown in Figure 9. At the beginning, the output voltage is 100 V with no load. A major disturbance corresponds with the minimum switching frequency and triggers a control function. The switching frequency is changed to the peak value and the output current is regulated to the desired value. The converter becomes stable again compared with Figure 4.

As shown in Figure 9, the output voltage can reach the desired value in 25 ms, which is sufficiently fast. The output voltage falls due to large loads. The switching frequency rises to the peak value during the trigger controlling process. Then the switching frequency is regulated by the conventional PI controller from minimum value to the desired value.

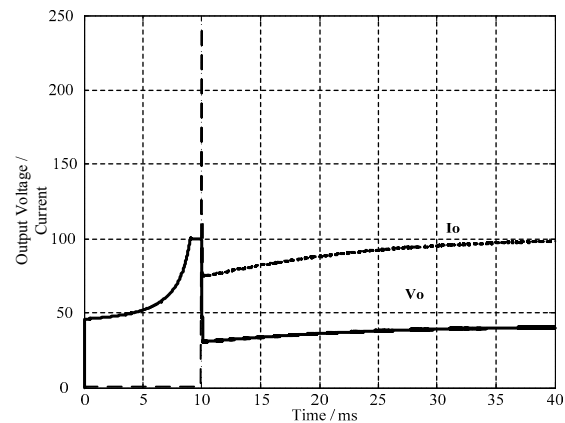


Figure 9. Output voltage and current of LLC converter with the proposed trigger control scheme.

## 5. Experiment Verification

In order to verify the correctness of the stability analysis, a full bridge LLC resonant converter prototype has been built. The parameters used for the model are given in Table 1.

Table 1. Parameters of the LLC resonant converter.

Parameter	Symbol	Value
Input Voltage (V)	$v_{in}$	100
Output Voltage (V)	$v_o$	24
Maximum Output Current (A)	$i_o$	8
Resonant Inductor ( $\mu\text{H}$ )	$L_r$	82
Resonant Capacitor (nF)	$C_r$	19
Magnetic Inductor ( $\mu\text{H}$ )	$L_m$	241.34
Transformer Ratio	$n$	10:1:1
Output Capacitor ( $\mu\text{F}$ )	$C$	3960

Based on the analysis in Sections 2 and 3, the frequency range has an important influence on the converter's stability. The peak frequency can be calculated as 66.41 kHz. In order to verify the stability criterion, two cases with different frequency ranges and controller parameters for LLC resonant converter are shown in Table 2.

Table 2. Two cases of different ranges for the LLC resonant converter.

No.	Frequency	$k_p$	$\tau (k_p/i_i)$	Equation (33)
1	70–300 kHz	−0.5	0.01	Yes
2		−1	0.01	Yes
3		−5	0.01	Yes
4		−10	0.01	Yes
5	50–300 kHz	−0.1	0.01	No
6		−0.5	0.01	No
7		−1	0.01	No
8		−5	0.01	No

Case 1 (No. 1–4): The compensation parameters are shown in Table 2. The frequency range of the LLC resonant converter is 70–300 kHz. The lower frequency is larger than the peak frequency of 66.41 kHz. The controller parameters are negative. They can satisfy Equation (33). Figures 10–13 give the voltage and current responses with different compensation parameters under full and half step loads. As the compensation parameters become larger and larger, the dynamic response of the LLC resonant converter becomes faster and faster. Under half step loads, the settling time is reduced from 45 ms to 8 ms and the voltage is reduced from 8.4 V to 1.2 V, with  $k_p$  rising from  $-0.5$  to  $-10$ . Similarly, under full step loads, the settling time is reduced from 47 ms to 8.8 ms and the voltage drop is reduced from 10 V to 1.6 V. Since the compensation parameters can satisfy the stability criterion, the converter can operate stably during a major disturbance, even with large compensation parameters of  $-10$ .

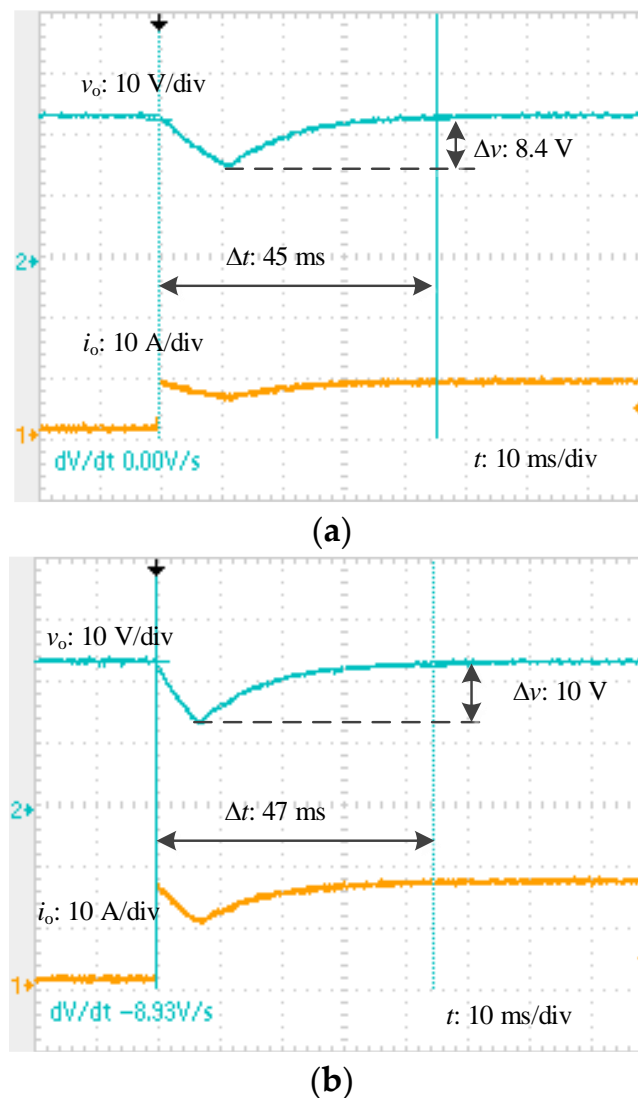
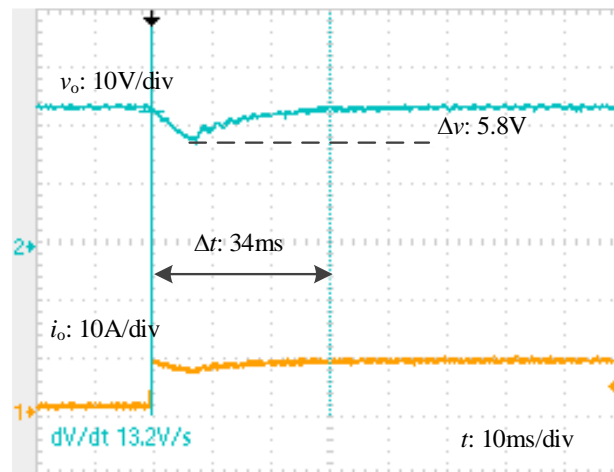
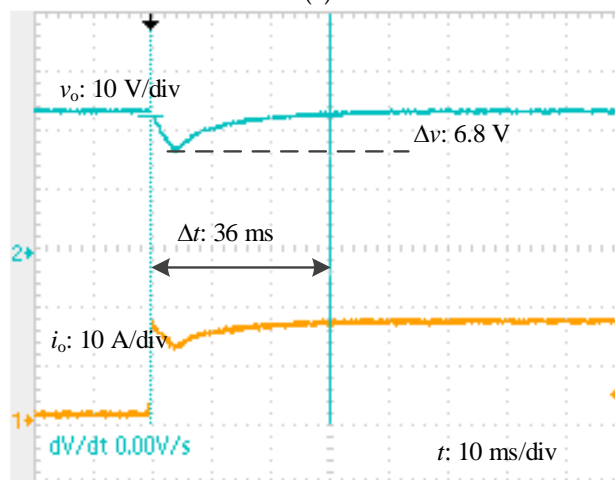


**Figure 10.** Waveforms of output voltage and current with Case 1: (a) Step from light to half; (b) step from light to full.

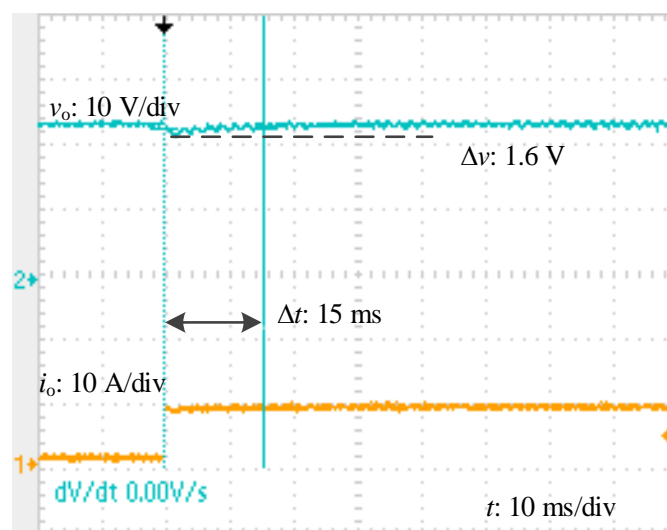


(a)



(b)

**Figure 11.** Waveforms of output voltage and current with Case 2: (a) Step from light to half; (b) step from light to full.



(a)

**Figure 12.** Cont.

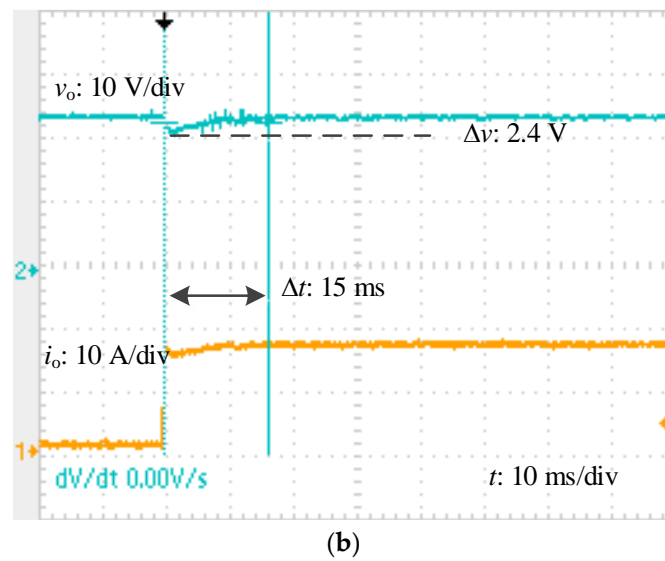


**Figure 12.** Waveforms of output voltage and current with Case 3: (a) Step from light to half; (b) step from light to full.

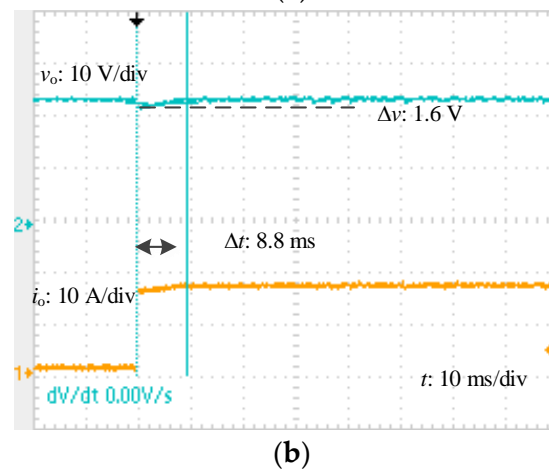
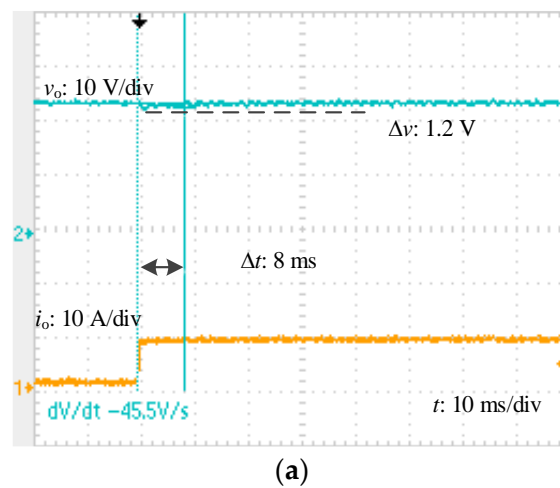


**Figure 13.** Waveforms of output voltage and current with Case 4: (a) Step from light to half; (b) step from light to full loads.

Case 2 (No. 5–8): The frequency range of LLC resonant converter is 50–300 kHz. The frequency is smaller than the peak frequency of 66.41 kHz. With large compensation parameters and disturbance, the frequency may be kept lower than 66.41 kHz during the controlling process. Then the converter cannot satisfy the stable criterion and may be unstable. However, with small compensation parameters and minor disturbance, the frequency should always be larger than 66.41 kHz during the regulating process. The system can satisfy Equation (33) and be stable during the regulation process. Figures 14–17 give the voltage and current response with different compensation parameters under full and half step loads. As the compensation parameters become larger and larger, the LLC resonant converter becomes more and more unstable. When the compensation parameters are small, the LLC resonant converter can be stable during a more major disturbance, as shown in Figures 14 and 17. When the compensation parameter is increased to  $-5$ , the converter cannot operate stably during a disturbance, as shown in Figure 17. The voltage is maintained at 16.8 V at half loads and 12 V at full loads. The frequency is regulated to 50 kHz due to the saturation, and the converter is unstable. When the converter has the same compensation parameters, a more major disturbance makes the converter more unstable, as shown in Figure 16. When the compensation parameter is  $-1$ , the LLC resonant converter is stable at half step loads and unstable at full step loads. Due to a major disturbance, the frequency remains smaller than 66.41 kHz during the controlling process at full step loads. Then the converter becomes unstable and the output voltage is maintained at 12 V. When the frequency in the saturation is kept smaller than the peak frequency, the converter may be unstable at large compensation parameters and disturbance.

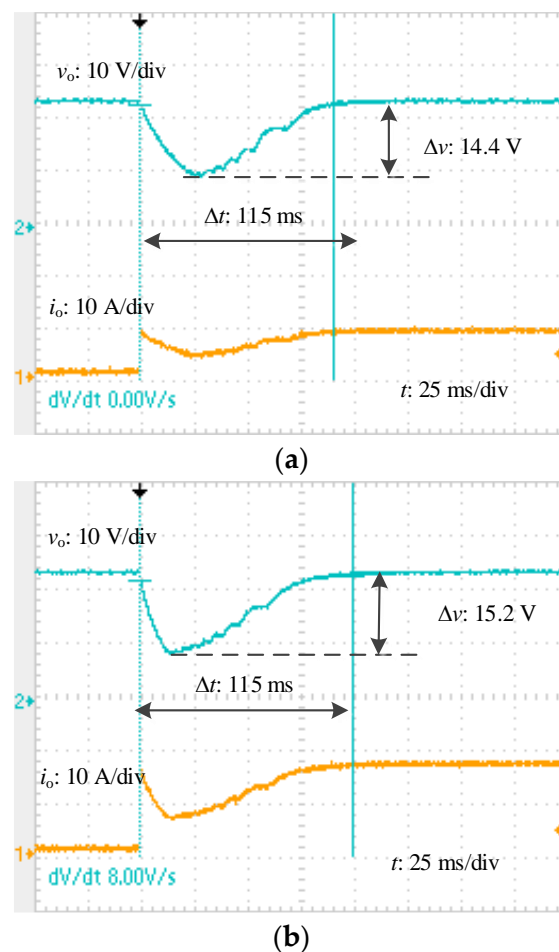
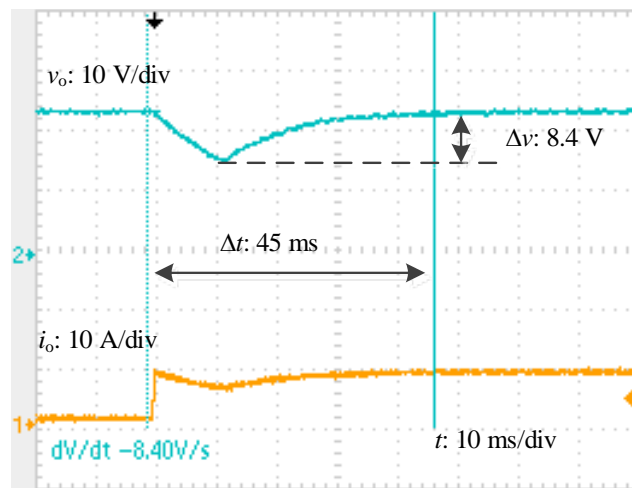
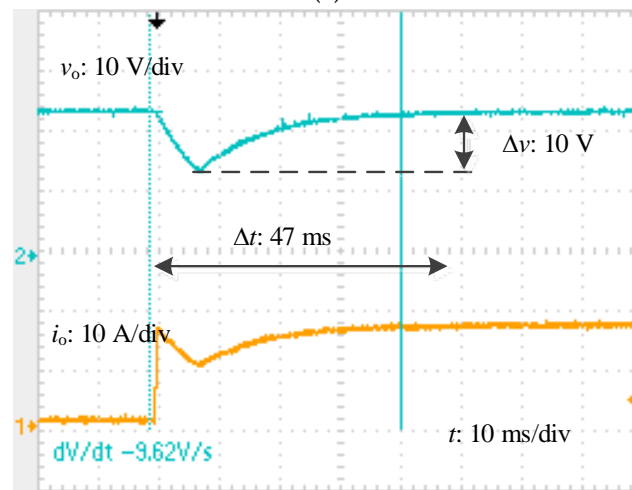


**Figure 14.** Waveforms of output voltage and current with Case 5: (a) Step from light to half; (b) step from light to full.

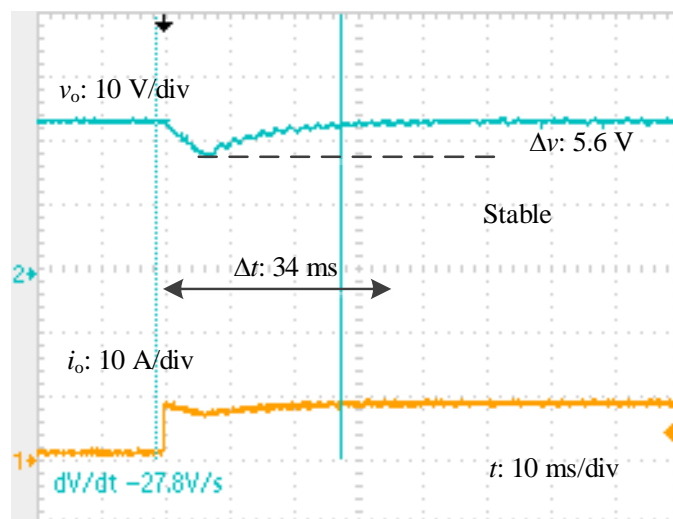


(a)



(b)

**Figure 15.** Waveforms of output voltage and current with Case 6: (a) Step from light to half; (b) step from light to full.



(a)

**Figure 16.** Cont.

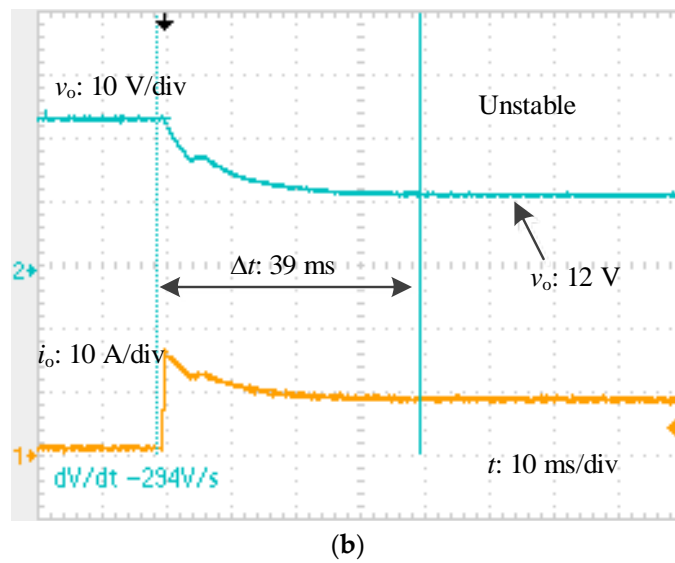


**Figure 16.** Waveforms of output voltage and current with Case 7: (a) Step from light to half; (b) step from light to full.

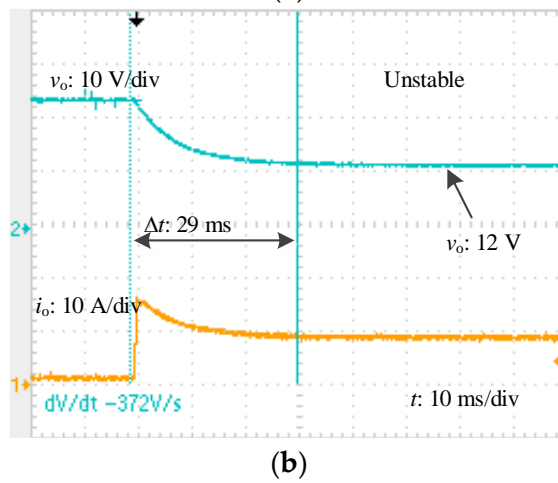
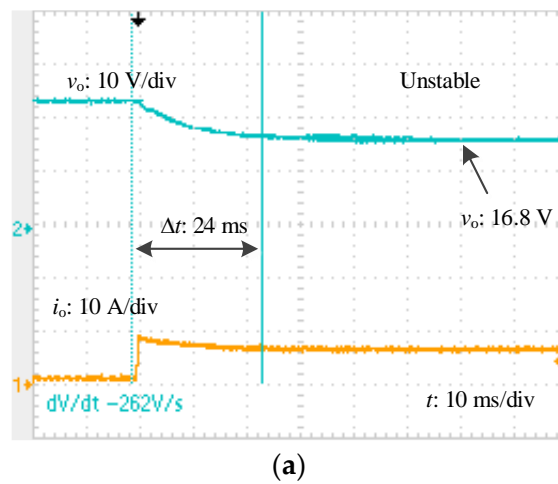
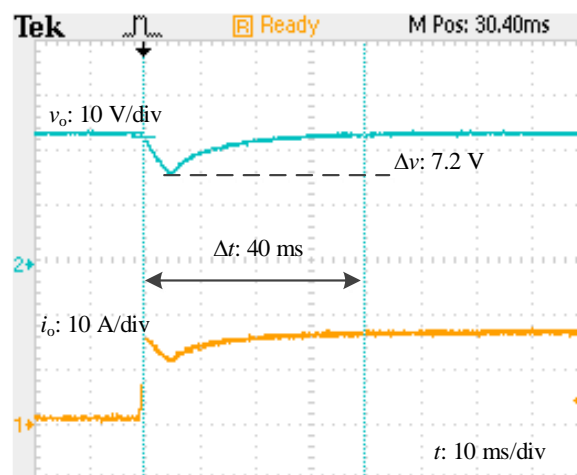


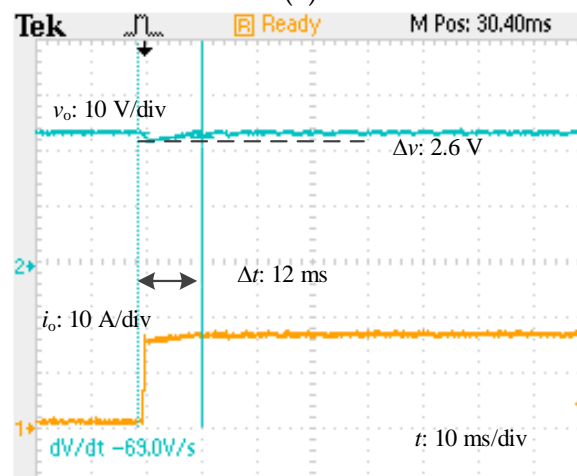
**Figure 17.** Waveforms of output voltage and current with Case 8: (a) Step from light to half; (b) step from light to full.

When the frequency in the saturation is larger than the peak frequency, the converter can satisfy the stability criterion even at large compensation parameters. The converter can be stable at full step loads with a large compensation value ( $k_p = -10$ ), as shown in Figure 13. If the saturation does not limit the minimum frequency, the frequency cannot satisfy the stable criterion during the regulation process; on the contrary, the converter is unstable at full step loads even with a small compensation value of  $-1$ , as shown in Figure 16b. When the compensation parameters are small enough, the converter can satisfy the stability criterion during the regulation process. The converter has the same dynamic response for both cases, as shown in Figures 10 and 15. They are both stable. Therefore, if the converter satisfies the stability criterion in Equation (33), the converter can be stable under any disturbance conditions.

When the trigger control scheme is used, the LLC resonant converter becomes stable in both Cases 7 and 8, as shown in Figure 18. When the loads change from light to full, the switching frequency is controlled to 50 kHz at the beginning, operating at the capacitive area. The CPD controller detects the positive current and sends a signal to the PI controller, which will force the switching frequency to the peak frequency of 70 kHz. Then the converter will be stable and the output voltage can be regulated to the desired value. The dynamic response with trigger controller in Cases 7 and 8 is similar to that in Cases 2 and 3 since they have the same controlling parameters. Therefore, the trigger controller can effectively extend the operational range of the LLC resonant converter.



(a)



(b)

**Figure 18.** Waveforms of output voltage and current with trigger controller against step loads from light to full: (a) No 7; (b) No 8.

## 6. Conclusions

In this paper, the instability performance of an LLC resonant converter during a major disturbance is analyzed and a trigger controller is expressed to extend the converter's operational range. Both qualitative and theoretical analysis demonstrate that system stability performance is highly dependent on the operating range of the switching frequency, in that there is a critical value determining the stability boundary. The regulated switching frequency should be higher than the critical frequency to ensure the stability of the system, or the converter will fall into instability. The same result is also obtained from a mathematical point of view by the utilization of the mixed potential function method. A trigger controller is also proposed and designed. By detecting the resonant currents' polarity, the switching frequency is forced to the peak frequency, preventing the converter from operating in the capacitive area. The investigation results and proposed controller presented in this paper provide a useful guideline for the LLC resonant converter design: the switching frequency range must be higher than the peak frequency to ensure the stability of the converter.

**Acknowledgments:** This work was supported in part by the National Natural Science Foundation of China under Project 51707138, and in part by the National Natural Science Foundation of China under Project 51507114.

**Author Contributions:** Zhijian Fang and Junhua Wang conceived and designed the experiments; Guozheng Hu and Jianwei Shao performed the experiments; Zhijian Fang and Shanxu Duan analyzed the data; Junhua Wang and Shanxu Duan contributed reagents/materials/analysis tools; Zhijian Fang wrote the paper.

**Conflicts of Interest:** The authors declare no conflict of interest.

## References

1. An, L.; Lu, D.D.C. Analysis of DC Bus Capacitor Current Ripple Reduction in Basic DC/DC Cascaded Two-Stage Power Converters. *IEEE Trans. Ind. Electron.* **2016**, *63*, 7467–7477. [[CrossRef](#)]
2. Kathiresan, R.; Das, P.; Reindl, T.; Panda, S.K. A Novel ZVS DC-DC Full-Bridge Converter with Hold-Up Time Operation. *IEEE Trans. Ind. Electron.* **2017**, *64*, 4491–4500. [[CrossRef](#)]
3. Kang, S.W.; Cho, B.H. Digitally Implemented Charge Control for LLC Resonant Converters. *IEEE Trans. Ind. Electron.* **2017**, *64*, 6159–6168. [[CrossRef](#)]
4. Kundu, U.; Yenduri, K.; Sensarma, P. Accurate ZVS Analysis for Magnetic Design and Efficiency Improvement of Full-Bridge LLC Resonant Converter. *IEEE Trans. Power Electron.* **2017**, *32*, 1703–1706. [[CrossRef](#)]
5. Jensen, S.; Maksimovic, D. Fast Tracking Electrosurgical Generator Using Two-Rail Multiphase Buck Converter With GaN Switches. *IEEE Trans. Power Electron.* **2017**, *32*, 634–641. [[CrossRef](#)]
6. Nemchinsky, V. Erosion of Thermionic Cathodes in Welding and Plasma Arc Cutting Systems. *IEEE Trans. Plasma Sci.* **2014**, *42*, 199–215. [[CrossRef](#)]
7. Lu, Y.; Wu, Q.; Wang, Q.; Liu, D.; Xiao, L. Analysis of a Novel Zero-Voltage-Switching Bidirectional DC/DC Converter for Energy Storage System. *IEEE Trans. Power Electron.* **2017**, *PP*, 1. [[CrossRef](#)]
8. Abeywardana, D.B.W.; Hredzak, B.; Agelidis, V.G. A Fixed-Frequency Sliding Mode Controller for a Boost-Inverter-Based Battery-Supercapacitor Hybrid Energy Storage System. *IEEE Trans. Power Electron.* **2017**, *32*, 668–680. [[CrossRef](#)]
9. Lu, Y.; Wu, H.; Sun, K.; Xing, Y. A Family of Isolated Buck-Boost Converters Based on Semiactive Rectifiers for High-Output Voltage Applications. *IEEE Trans. Power Electron.* **2016**, *31*, 6327–6340. [[CrossRef](#)]
10. Severns, R.P. Topologies for three-element resonant converters. *IEEE Trans. Power Electron.* **1992**, *7*, 89–98. [[CrossRef](#)]
11. Fang, Z.; Wang, J.; Duan, S.; Liu, K.; Cai, T. Control of an LLC Resonant Converter Using Load Feedback Linearization. *IEEE Trans. Power Electron.* **2017**, *PP*, 1. [[CrossRef](#)]
12. Haga, H.; Kurokawa, F. Modulation Method of a Full-Bridge Three-Level LLC Resonant Converter for Battery Charger of Electrical Vehicles. *IEEE Trans. Power Electron.* **2017**, *32*, 2498–2507. [[CrossRef](#)]
13. Yang, B.; Lee, F.C.; Zhang, A.J.; Guisong, H. LLC resonant converter for front end DC/DC conversion. In Proceedings of the APEC Seventeenth Annual IEEE Applied Power Electronics Conference and Exposition, Dallas, TX, USA, 10–14 March 2002; Volume 2, pp. 1108–1112.

14. Navarro-Crespin, A.; Casanueva, R.; Azcondo, F.J. Performance Improvements in an Arc-Welding Power Supply Based on Resonant Inverters. *IEEE Trans. Ind. Appl.* **2012**, *48*, 888–894. [[CrossRef](#)]
15. Buccella, C.; Cecati, C.; Latafat, H.; Pepe, P.; Razi, K. Observer-Based Control of LLC DC/DC Resonant Converter Using Extended Describing Functions. *IEEE Trans. Power Electron.* **2015**, *30*, 5881–5891. [[CrossRef](#)]
16. Fang, Z.; Cai, T.; Duan, S.; Chen, C. Optimal Design Methodology for LLC Resonant Converter in Battery Charging Applications Based on Time-Weighted Average Efficiency. *IEEE Trans. Power Electron.* **2015**, *30*, 5469–5483. [[CrossRef](#)]
17. Yang, B.; Lee, F.C.; Jovanovic, M. Small-signal analysis for LLC resonant converter. In Proceedings of the CPES Seminar, Blacksburg, VA, USA, 27–29 April 2003; pp. 144–149.
18. Chang, C.H.; Chang, E.-C.; Cheng, C.-A.; Cheng, H.-L.; Lin, S.-C.L. Small Signal Modeling of LLC Resonant Converters Based on Extended Describing Function. In Proceedings of the 2012 International Symposium on Computer, Consumer and Control (IS3C), Taichung, Taiwan, 4–6 June 2012; pp. 365–368.
19. Cheng, B.; Musavi, F.; Dunford, W.G. Novel small signal modeling and control of an LLC resonant converter. In Proceedings of the 2014 Twenty-Ninth Annual IEEE Applied Power Electronics Conference and Exposition (APEC), Fort Worth, TX, USA, 16–20 March 2014; pp. 2828–2834.
20. Stahl, J.; Steuer, H.; Duerbaum, T. Discrete modeling of resonant converters Steady state and small signal description. In Proceedings of the 2012 IEEE Energy Conversion Congress and Exposition (ECCE), Raleigh, NC, USA, 15–20 September 2012; pp. 1578–1584.
21. Jang, J.; Joung, M.; Choi, S.; Choi, Y.; Choi, B. Current mode control for LLC series resonant dc-to-dc converters. In Proceedings of the 2011 Twenty-Sixth Annual IEEE Applied Power Electronics Conference and Exposition (APEC), Fort Worth, TX, USA, 6–11 March 2011; pp. 21–27.
22. Jang, J.; Kumar, P.S.; Kim, D.; Choi, B. Average current-mode control for LLC series resonant dc-to-dc converters. In Proceedings of the 2012 7th International Power Electronics and Motion Control Conference (IPEMC), Harbin, China, 2–5 June 2012; pp. 923–930.
23. Zong, S.; Luo, H.; Li, W.; He, X.; Xia, C. Theoretical Evaluation of Stability Improvement Brought by Resonant Current Loop for Paralleled LLC Converters. *IEEE Trans. Ind. Electron.* **2015**, *62*, 4170–4180. [[CrossRef](#)]
24. Feng, W.; Lee, F.C. Optimal Trajectory Control of LLC Resonant Converters for Soft Start-Up. *IEEE Trans. Power Electron.* **2014**, *29*, 1461–1468. [[CrossRef](#)]
25. Feng, W.; Lee, F.C.; Mattavelli, P. Optimal Trajectory Control of LLC Resonant Converters for LED PWM Dimming. *IEEE Trans. Power Electron.* **2014**, *29*, 979–987. [[CrossRef](#)]
26. Zahid, Z.U.; Lai, J.S.J.; Huang, X.K.; Madiwale, S.; Hou, J. Damping impact on dynamic analysis of LLC resonant converter. In Proceedings of the 2014 Twenty-Ninth Annual IEEE Applied Power Electronics Conference and Exposition (APEC), Fort Worth, TX, USA, 16–20 March 2014; pp. 2834–2841.
27. Verghese, G.C.; Elbuluk, M.E.; Kassakian, J.G. A General Approach to Sampled-Data Modeling for Power Electronic Circuits. *IEEE Trans. Power Electron.* **1986**, *PE-1*, 76–89. [[CrossRef](#)]
28. Du, W.; Zhang, J.; Zhang, Y.; Qian, Z. Stability Criterion for Cascaded System with Constant Power Load. *IEEE Trans. Power Electron.* **2013**, *28*, 1843–1851. [[CrossRef](#)]
29. Jeltsema, D.; Scherpen, J.M.A. On Brayton and Moser’s missing stability theorem. *IEEE Trans. Circuits Syst. II: Express Briefs* **2005**, *52*, 550–552. [[CrossRef](#)]

